

## Research Article

# Development of a Method for Enhanced Fan Representation in Gas Turbine Modeling

Georgios Doulgeris,<sup>1</sup> Hossein Khaleghi,<sup>1</sup> Anestis Kalfas,<sup>2</sup> and Pericles Pilidis<sup>1</sup>

<sup>1</sup>Department of Power and Propulsion, SOE, Cranfield University, Bedfordshire MK43 0AL, UK

<sup>2</sup>Department of Mechanical Engineering, Aristotle University of Thessaloniki, 54124 Thessaloniki, Greece

Correspondence should be addressed to Georgios Doulgeris, g.doulgeris@cranfield.ac.uk

Received 1 November 2010; Revised 11 May 2011; Accepted 17 May 2011

Academic Editor: M. Razi Nalim

Copyright © 2011 Georgios Doulgeris et al. This is an open access article distributed under the Creative Commons Attribution License, which permits unrestricted use, distribution, and reproduction in any medium, provided the original work is properly cited.

A challenge in civil aviation future propulsion systems is expected to be the integration with the airframe, coming as a result of increasing bypass ratio or above wing installations for noise mitigation. The resulting highly distorted inlet flows to the engine make a clear demand for advanced gas turbine performance prediction models. Since the dawn of jet engine, several models have been proposed, and the present work comes to add a model that combines two well-established compressor performance methods in order to create a quasi-three-dimensional representation of the fan of a modern turbofan. A streamline curvature model is coupled to a parallel compressor method, covering radial and circumferential directions, respectively. Model testing has shown a close agreement to experimental data, making it a good candidate for assessing the loss of surge margin on a high bypass ratio turbofan, semiembedded on the upper surface of a broad wing airframe.

## 1. Introduction

Gas turbine off-design performance is broadly predicted through zero dimensional analysis methods [1–3]. Such methods are based on discrete component maps that treat every engine component as black box operating under averaged fluid values, such as mass flow, temperature, and pressure. A drawback in such approach is poor response to flow nonuniformities, which can be of critical importance in predicting engine performance under inlet distortion.

Since late 1950s, gas turbine engineers realized the severity of inlet distortion effects on engine performance. As a result, several experimental and computational studies focused on the assessment of inlet distortion. The work of Lieblein [4] was one example of experimental research on the inception of surge on compressor blades. Later on, the attenuation of circumferential flow distortion, through multistage compressors, was studied by Plourde [5], while Callahan and Stenning [6] presented experimental and theoretical results on the attenuation of distortion upstream the compressor.

In the area of numerical models, the parallel compressor was firstly proposed by Pearson and McKenzie [7]. The capabilities of the parallel compressor were further investigated by Reid [8], who showed the effect of spoiled area angle on compressor surge margin and the deviation between experimental and theoretical results. Following this, he identified the critical distortion angle ( $\theta_{crit}$ ), above which, surge margin loss reduces significantly.

During the 1970s, significant research was undertaken by NASA. The effect of circumferential distortion on gas turbine performance was investigated by Calogeras et al. [9] and Milner and Wenzel [10], who presented the operating line shift of a J85-GE-13 turbojet, under various distortion patterns. The stability of the same engine under combined inlet temperature and pressure distortion was consequently studied by Braithwaite et al. [11]. In the same study the application of a parallel compressor model showed a reasonable agreement with the experiment.

The parallel compressor method was used as the basis of extended models. One example was the paper from Greitzer and Griswold [12] that included analytical expressions of

compressor stability and compressor-diffuser interaction. The main focus, though shifted to the study of compressor dynamic response, and several models were proposed in the area [13–15].

Even though most of past research focused on circumferential distortion, significant work on the effect of radial perturbations was undertaken in Cranfield University. Yin and Pilidis [16] and Yin et al. [17] have proposed a two-dimensional turbofan model for the calculation of engine performance under radial inlet profiles, based on experimentally derived fan maps. A different approach was followed by Pachidis et al. [18], who proposed a 2D streamline curvature method for compressor performance. Input to this model were inlet radial profiles, used in coupling the CFD simulation of an axisymmetric intake with a gas turbine performance code [19]. The present work provides an enhancement to the prediction method, by extending the streamline curvature to quasi-3D, through coupling parallel compressor theory with streamline curvature.

## 2. Enhanced Fan Model

An enhanced quasi-3D fan representation is proposed combining a streamline curvature model (in the radial direction) with a multiple parallel compressor method (in the circumferential direction), in order to capture three-dimensional effects of a highly distorted inlet flow. The core of the model is the streamline curvature model, controlled by the parallel compressor model as shown in Figures 1 and 2.

**2.1. Parallel Compressor Theory.** The rationale of the parallel compressor (PC) model is the split of the compressor into two separate virtual compressor segments. Both of these segments operate under the same rotational speed and discharge to a common plenum. Their main difference, though, is the inlet condition; one segment operates under clean inlet flow (area averaged total pressure on the “clean” sector), while the second one is subjected to low inlet pressure (area averaged total pressure  $P_t$  on the “spoiled” sector).

The exit boundary condition for the two compressor segments is the discharge to a common plenum. As a result, exit static pressure and flow angle are the same for both sectors, as no mixing is assumed. Such an assumption is valid, due to the presence of stator blades, which are designed for creating uniform exit flow conditions, while it is established by several experimental studies, such as the one from Sanger, [20]. In this study, very low deviation of static pressure was shown at the fan exit plane

$$m_i = \frac{Q_i P_{ti}}{\sqrt{T_{ti}}} \cdot \frac{\theta_i}{360^\circ}. \quad (1)$$

Under the condition of common rotational speed, the “clean” segment operates at higher mass flow and lower pressure in order to match the low exit static pressure of the “distorted” sector. The mass flow is calculated using (1), where  $Q_i$  is the nondimensional mass flow of the corresponding parallel sector. In a further step, overall compressor performance is calculated after appropriate averaging

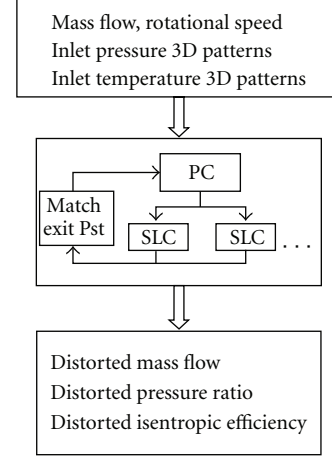


FIGURE 1: Enhanced parallel compressor model.

between the two sectors. Exit  $P_t$  and mass flow are defined by area averaging (2) and (3), while  $T_t$  by mass averaging (4). Term “ $\theta$ ” is the sector angle of each sector (5) and represents annulus area due to circumferentially constant radius

$$P_t = \frac{\theta_1 P_{t1} + \theta_2 P_{t2}}{360^\circ}, \quad (2)$$

$$m = m_1 + m_2, \quad (3)$$

$$T_t = \frac{m_1 T_{t1} + m_2 T_{t2}}{m}, \quad (4)$$

$$\theta_1 + \theta_2 = 360^\circ. \quad (5)$$

The parallel compressor method has been broadly used for defining the surge limit of a compressor. In this process, the surge limit of the “clean” speed line is assumed to be common for both “clean” and “distorted” sectors. As a result, surge occurs when surge limit is reached at the “distorted” sector, and the averaged values of  $P_t$  and non-dimensional mass flow give the “distorted” surge limit. This surge criterion has been broadly used in bibliography, such as [21, 22]. It is based on the assumption of using the same non-dimensional map for both sectors and allows the qualitative assessment of surge margin loss.

**2.2. Parallel Compressor Performance and Enhancement.** The performance of a conventional parallel compressor model can be summarized in Figure 2, where the effect of magnitude of distortion—expressed as the difference between distorted and clean sectors—on surge pressure ratio and mass flow is illustrated. Inlet distortion has a linear effect on loss in surge pressure ratio. The reason can be traced in the direct impact of inlet total pressure to exit static pressure, as “distorted” sector pressure ratio equals the surge pressure ratio during the whole process. As a result, any loss of total pressure due to inlet distortion in the “distorted” sector is matched by a loss in pressure ratio in the “clean” one, with the linear effect shown in Figure 2. On the other hand, a nonlinear behavior is exhibited in terms of compressor mass flow. “Clean” sector pressure ratio is associated with

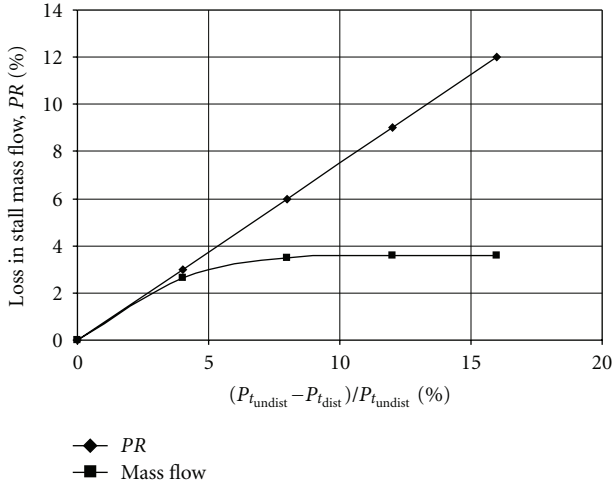


FIGURE 2: Conventional PC compressor response to distortion.

non dimensional mass flow through the shape and gradient of the compressor speed line under consideration. As a result, choking of the compressor at low pressure ratio does not allow linear increase of the mass flow, as illustrated in Figure 2. It should be, therefore, highlighted that parallel compressor results are dependent on the shape of the map characteristics under consideration.

In addition to distortion magnitude, the area of the distorted sector has a critical effect on the performance prediction of the model, as discussed by Longley and Greitzer, [23] and Reid, [8]. This attribute is clearly depicted in Figure 3, where parallel compressor prediction is compared to experimental data provided by Reid, [8]. What becomes apparent is the existence of a critical angle. For extent of distortion, lower than this angle, the negative effect on surge pressure ratio diminishes in contrast to the prediction of conventional parallel compressor theory. The reason is that parallel compressor presents a linear relation between the extent of spoiled sector and surge pressure ratio loss, as this is the result of area averaging between the two compressors. In order to reduce this overprediction of surge pressure ratio loss, a correction is suggested, based on the critical angle " $\theta_{crit}$ ", which in the case of Figure 3 appears to be set at  $90^\circ$ . This correction affects the averaging between the circumferential sectors. As a result, the sector angle of the most spoiled sector is modified according to (6).

The implementation of (6) enables the modelling of narrow distorted areas and, thus, the use of more than two circumferential sectors, where applicable. As a result, the number of circumferential sectors can vary

$$\begin{aligned} \theta'_{dist} &= \theta_{crit} + (\theta_{crit} - \theta'_{dist}) \quad \text{for } \theta_{dist} < \theta_{crit}, \\ \theta'_{dist} &= \theta_{crit} \quad \text{for } \theta_{dist} > \theta_{crit}. \end{aligned} \quad (6)$$

Another modification on the parallel compressor is related to the extension of the model to predict distortion amplification downstream the fan due to varying fan exhaust duct area. This model uses  $Q$ -function at the stator exit and

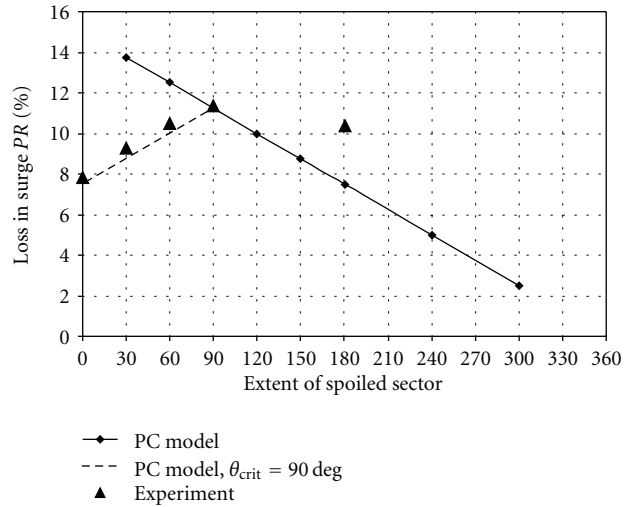


FIGURE 3: Conventional and corrected PC models against experimental data from [8].

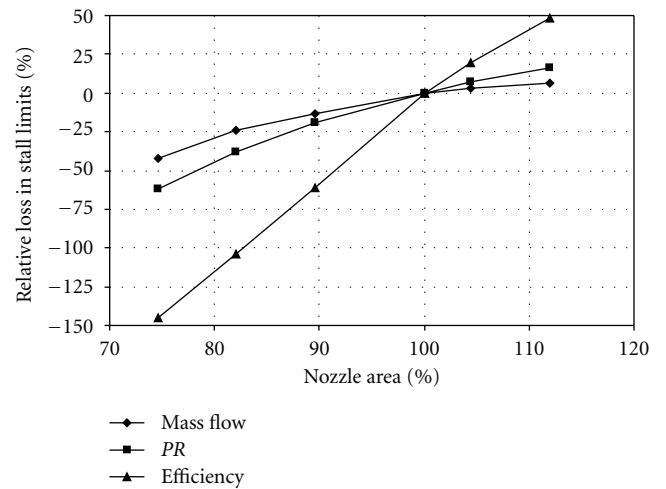


FIGURE 4: Effect of variable nozzle on loss in surge mass flow, PR, and efficiency.

nozzle exit, having as input the area ratio between these two stations. Figure 4 illustrates the effect of varying fan exhaust area on loss in surge margin. The use of a convergent nozzle duct with exit area 80% of fan exit leads to  $\sim 50\%$  improvement in surge loss for PR,  $\sim 25\%$  for mass flow and  $\sim 100\%$  for isentropic efficiency. As a result, fan stability can benefit from a converging exhaust duct, while the installation of this model in a gas turbine performance code can enable the evaluation of variable nozzle on overall engine stability.

The parallel compressor model includes the inherent assumption of no cross-flow between the parallel segments. To accommodate this and reduce the sensitivity of parallel segments to extended areas of distortion, the maximum number of parallel segments has been set at 4. Moreover,

as discussed by Longley and Greitzer, [23], this assumption allows the generation of realistic results.

**2.3. Streamline Curvature Model.** The core of this distortion prediction method is the streamline curvature (SLC) compressor model, developed by Pachidis [24] and Templalexis, [25]. This model creates the compressor characteristics, using as input geometrical, aerodynamic, and thermodynamic data along the radial direction. In such way, higher fidelity is achieved through analysing the effect of radial distortion inlet patterns on compressor performance.

The SLC is an inviscid through-flow analysis method, in which empirical correlations are used to account for viscous losses. The equations implemented in the model are based on axisymmetric, compressible, inviscid flow through a compressor. As a result, the law of conservation of angular momentum (7) includes terms for pressure forces, derivative of velocity, centripetal acceleration, and coriollis acceleration. Furthermore, the gradient of meridional velocity is calculated from the full radial equilibrium equation (8), which is derived from(7)

$$-\frac{1}{\rho} \nabla P = \frac{DW}{Dt} + \omega \times \omega \times r + 2\omega \times W + F, \quad (7)$$

$$\frac{\partial V_m^2}{\partial s} = V_m^2 2 \cos^2 \alpha$$

$$\times \left[ \begin{array}{l} \frac{\cos(\varepsilon + \gamma)}{R_c} - \frac{\tan \alpha (\partial \alpha / \partial s)}{\cos^2 \alpha} + \sin(\varepsilon + \gamma) \\ \times \left( -\frac{1}{\cos(\varepsilon + \gamma)} \frac{\partial \varepsilon}{\partial s} + \frac{\tan(\varepsilon + \gamma)}{R_c} - \frac{\partial \ln(r_p)}{\partial m} \right) \end{array} \right] + 2 \cos^2 \alpha \left( \frac{\partial I}{\partial s} - 2 \cos \gamma \omega (V_w - U) - T \frac{\partial S}{\partial s} \right), \quad (8)$$

$$m_j = \int \bar{\rho}_j \bar{V}_{m_j} dA. \quad (9)$$

The meridional velocity is calculated by solving the above equation, with mass continuity as constraint. Equations (8) and (9) are solved iteratively. After a first guess of the curvature of the streamlines, the radial distribution of the meridional velocity at the blade leading edge is calculated. Taking into account blade geometry, the velocity triangles, entropy, and enthalpy rise are calculated, and the meridional velocity distribution at blade trailing edge is used for establishing the mass flow in order to check for continuity. The iterations are based on mass flow convergence, while the streamtube mass flow is used to determine the radial position of each streamline.

Isentropic efficiency calculation is based on the calculation of entropy generation along each streamline due to

nonisentropic compression. Pressure losses are defined as function of pressure loss coefficient that includes blade profile losses, shock losses, and secondary losses (for the rotor). Profile losses and shock losses are calculated according to [26], while secondary losses are calculated according to [27].

The SLC model has been validated [24, 25] against published data, [28, 29], and good quantitative and qualitative agreement between measured and SLC results has been shown, [18].

**2.4. Coupled Parallel Compressor Streamline Curvature (PC-SLC) Model.** The combination of parallel compressor theory with a streamline curvature method targets to provide an enhanced representation of a fan by incorporating radial and circumferential distortion patterns. In further detail, the nondimensional map is replaced by a streamline curvature fan model. As a result, during the parallel compressor iterative process, the operating point of every segment is calculated by the code instead of being result of map interpolation.

Typical input to the model is radial profiles of inlet total pressure and temperature for various circumferential positions. These profiles are fed to each circumferential parallel compressor segment, and Newton Raphson method is applied for matching exhaust static pressure (radially area averaged) for all sectors

$$K = \frac{\bar{P}_t - \bar{P}_{t,\text{distorted}}}{\bar{P}_t}. \quad (10)$$

The number of parallel sectors and the extent of spoiled sector are calculated in relation to the distortion index  $K$  (10). The distorted area “ $\theta_{\text{dist}}$ ” is the area at the aerodynamic inlet plane operating under inlet—radially area weighted—total pressure, lower than the averaged  $P_t$  of the whole annulus. Consequently, the number of segments is related to this minimum area; that is,  $\theta_{\text{dist}}$  of  $180^\circ$  does not allow for more than 2 circumferential sectors, while a  $45^\circ$  distorted area would allow for 8 segments.

### 3. Model Verification/Calibration

The streamline curvature method of the present study was validated in [24, 25] for uniform and radially distorted inlet flows. Additionally, validation of the parallel compressor model can be found in (7) and (8). A further comparison to measured data and choice of “ $\theta_{\text{crit}}$ ” can further enhance the confidence on the proposed model.

For the purposes of model verification, fan experimental data are compared with the model. The chosen fan is the NASA TP 1294 presented in [20]. However, due to lack of available geometric data, the input geometry to the streamline curvature method was based on the first stage of the NASA TP 1493 two-stage fan. A comparison between the two fans in Table 1 reveals the design similarities that make possible a direct comparison for the scope of a verification study that includes the comparison to results from conventional but also enhanced parallel compressor models.

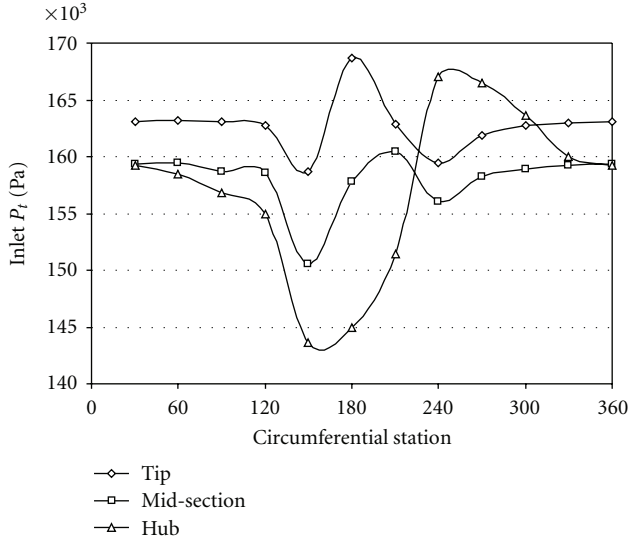


FIGURE 5: Inlet total pressure circumferential distribution, [20].

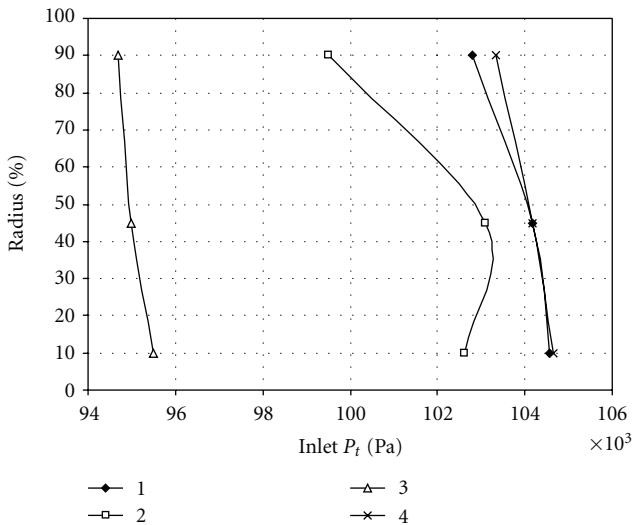


FIGURE 6: Radial profiles of inlet  $P_t$  for 4-sector parallel compressor.

The calibration of the model includes the investigation of the effect of the number of circumferential sectors, thus the extent of the distorted sector, in order to identify the critical angle of the fan. This angle is expected to be related with results closest to experimental data. The critical angle which is unique for every compressor is, therefore, defined as the one that gives best matching to measured data, as shown in Figure 3. In such way, the model is calibrated to the experimental results for further use, such as under computationally obtained inlet profiles.

Figure 5 illustrates total pressure inlet profiles at the aerodynamic inlet plane of the fan, as obtained from [20]. A region of step reduction of  $P_t$  can be noticed due to the presence of a  $90^\circ$ -extent screen upstream the fan inlet. The distorted area angle " $\theta_{dist}$ " equals to  $120^\circ$ , and the distortion index " $K$ " is calculated as 7.75%. The radial variation of

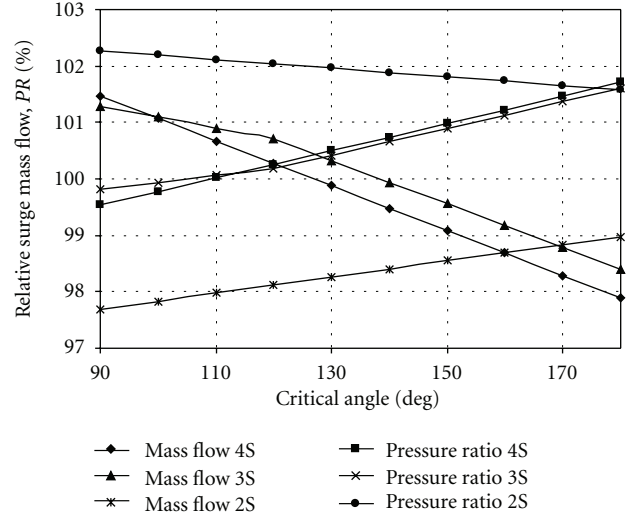


FIGURE 7: Effect of  $\theta_{crit}$  on surge mass flow and surge pressure ratio.

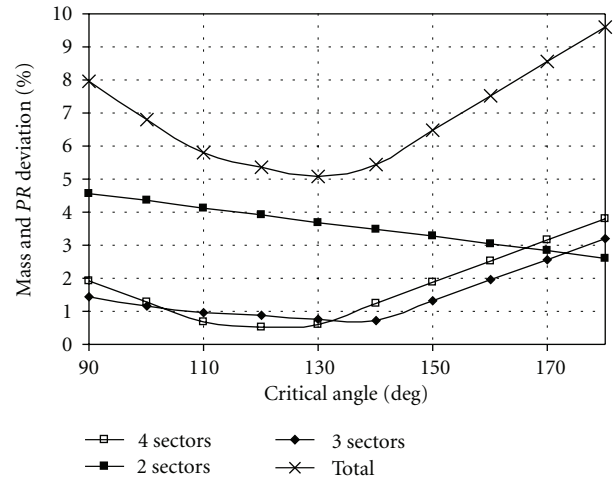


FIGURE 8: Deviation from experimental data versus " $\theta_{crit}$ ".

TABLE 1: Design point data of NASA TP1493 and NASA TP1294 fans.

|                       | NASATP 1493 | NASATP 1294 |
|-----------------------|-------------|-------------|
| Pressure ratio        | 1.59        | 1.574       |
| Temp. ratio           | 1.167       | 1.17        |
| Isentropic efficiency | 0.848       | 0.816       |
| Mass flow [kg/s]      | 33.248      | 29.484      |
| RPM                   | 16042.8     | 16100.0     |
| Tip speed [m/s]       | 428.9       | 424.6       |

total pressure is taken into consideration in the model, and  $P_t$  at each radial position is derived from circumferential area averaging. It is therefore, highly dependent on the number of circumferential sectors. A representative example is shown in Figures 6 and 7 for four circumferential sectors, where radial profiles have been generated for four 90 degree circumferential sectors.

A simple parallel compressor is used, with two or four circumferential segments, and area-weighted inlet total pressure for each segment, in order to serve as baseline. Additionally, several PC-SLC models using 2, 3, or 4 circumferential sectors are created, corresponding to sector angles of  $180^\circ$ ,  $120^\circ$ , and  $90^\circ$ , respectively. The use of various sector areas gives an insight into the performance of the PC-SLC. Moreover, constant inlet  $P_t$  distribution for each circumferential sector has been compared to radial distribution of  $P_t$ , in order to assess the effect of radial distortion on the solution. In a further step, the “ $\theta_{crit}$ ” correction is applied to be compared against the experimental data and the baseline.

The calibration process involves the identification of compressor critical angle, as discussed above. To achieve this, critical angle varies from  $90^\circ$  to  $180^\circ$ , and the correction is calculated according to (6). The resulting surge mass flow and pressure ratio are plotted in Figure 7, as percentage of the experimental values

$$(\Delta M \& \Delta PR) = \frac{M_{PC-SLC} - M_{Exp}}{M_{Exp}} + \frac{PR_{PC-SLC} - PR_{Exp}}{PR_{Exp}}. \quad (11)$$

It becomes apparent that increasing critical angle results in rising surge pressure ratio and reducing surge mass flow. It was, therefore, decided to express overall deviation as the sum of relative errors using (11). This approach resulted in a clear optimum region, as shown in Figure 8, where the sum of mass and pressure ratio deviations has been plotted against “ $\theta_{crit}$ ”. The critical angle chosen for the particular fan is the one exhibiting lowest total deviation from the experimental results for all created models, as illustrated in Figure 8. From this figure, total deviation from experimental data appears at “ $\theta_{crit}$ ” of  $130^\circ$ . This value is used in the comparison of the various models.

Total comparison to experimental data is included in Figures 9 and 10, where pressure ratio and change of efficiency  $\Delta(\text{efficiency})$  are plotted against corrected mass flow per unit area and several conclusions are extracted.

A comparison between “clean” speed lines shows good agreement between experimental and numerical results, especially in the near-surge region. This forms a solid basis for comparing the surge margin loss from the various models. As shown in Figure 9 the standard parallel compressor and the PC-SLC with and without radial distribution exhibit similar levels of surge pressure ratio loss. This is because radial distortion is relatively low compared to circumferential. On the other hand, the standard parallel compressor exhibits much lower levels of loss in efficiency, according to Figure 10, while efficiency prediction from PC-SLC is very close to the experimental result. Figure 9 shows, also, a significant difference between the 2-sector models and the rest. This happens due to the fact that the low-pressure sector is greater than the extent of circumferential distortion. As a result, the circumferentially averaged total pressure includes regions of higher pressure resulting in lower distortion (higher averaged values).

The implementation of “ $\theta_{crit}$ ” correction moves surge limit towards the experimental value, as it is clearly shown

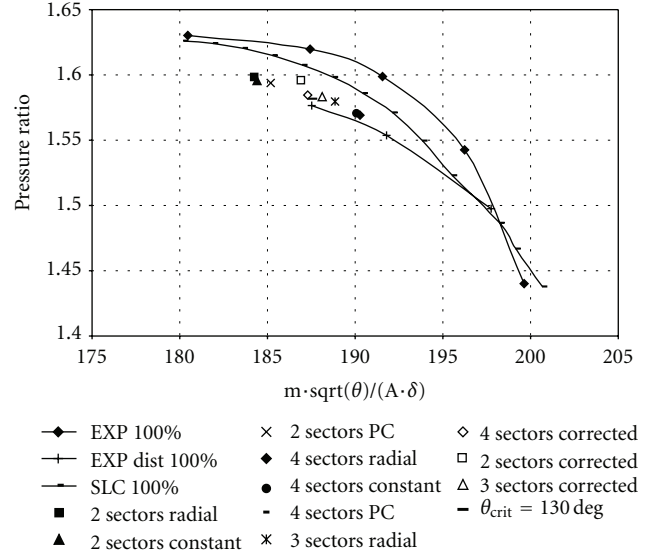


FIGURE 9: 100% speed line: pressure ratio theoretical and experimental results.

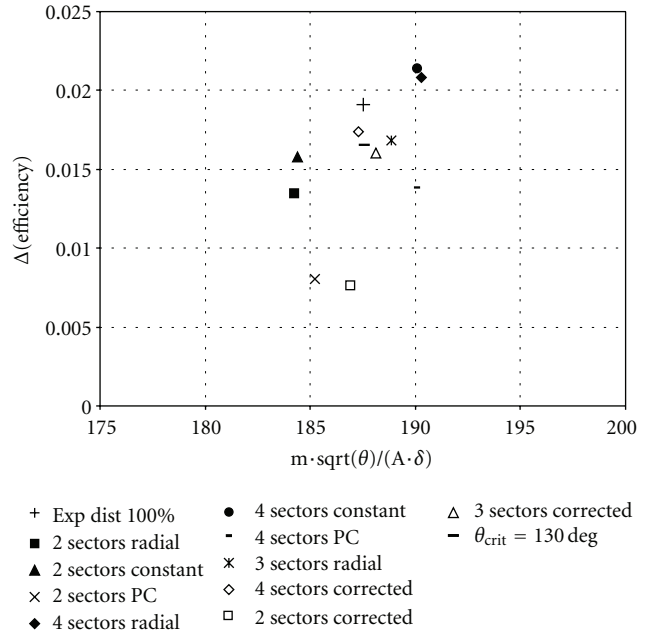


FIGURE 10: 100% speedline: isentropic efficiency increment theoretical and experimental results.

in Figures 9 and 10. Especially the models with 3 and 4 sectors (which include in one sector the whole region of low inlet pressure), when corrected, lay in the close proximity of the actual value of surge limit (pressure ratio mass flow and isentropic efficiency). This gives a strong confidence for using the PC-SLC model for the prediction of the effect of distortion on fan performance at least in a qualitative manner

$$\Delta(\text{efficiency}) = \frac{\eta_{clean} - \eta_{distorted}}{\eta_{clean}}. \quad (12)$$

## 4. Conclusions

A method has been proposed for assessing the effect of inlet distortion on the fan of an aeroengine through the coupling of a streamline curvature model with parallel compressor theory. Fan annulus is split to circumferential sectors according to parallel compressor theory, while each sector is modeled using streamline curvature method. In this way, the effect of highly nonuniform inlet flow patterns on fan performance can be assessed, enhancing the understanding of turbofan engine behavior under inlet distortion.

Critical angle is a unique parameter for every compressor. It is, therefore, essential that critical angle is chosen carefully due to the strong effect it has on the prediction of surge line shift.

The PC-SLC method is a performance assessment tool that can be integrated in a 0D gas turbine performance code. In this way, the analysis of engine response to inlet distortion can be achieved, enabling the gas turbine performance engineer evaluate installed engine performance from the stage of preliminary design.

## Nomenclature

A: Area [ $\text{m}^2$ ]  
M: Mass flow [ $\text{kg/s}$ ]  
P: Pressure [Pa]  
PR: Pressure ratio  
Q: Q-function, nondimensional mass flow  
T: Temperature [T]

## Greek

$\delta$ :  $P_t[\text{Pa}]/101325[\text{Pa}]$   
 $\theta$ : Sector angle  
 $\theta$ :  $T_t[\text{K}]/288.15[\text{K}]$

## Subscripts

clean: Undistorted, “clean”  
crit: Critical  
dist: Distorted, “spoiled”  
i: Inlet  
t: Total

## Superscripts

$\acute{\text{c}}$ : Corrected.

## References

- [1] P. Walsh and P. Fletcher, *Gas Turbine Performance*, Blackwell, 2nd edition, 2004.
- [2] H. I. H. Saravanamuttoo, G. F. C. Rogers, and H. Cohen, *Gas Turbine Theory*, Pearson Education, 5th edition, 2001.
- [3] J. D. Mattingly, W. H. Heiser, and D. T. Pratt, *Aircraft Engine Design*, AIAA Education Series, Reston, Va, USA, 2nd edition, 2002.
- [4] S. Lieblien, “Characteristics of two-dimensional compressor blade cascades,” NACA-RM-E 57A28, Washington, DC, USA, 1957.
- [5] G. A. Plourde, A. H. Stenning, U. Lehigh, and P. Bethlehem, “Attenuation of circumferential inlet distortion in multistage axial compressors,” *Journal of Aircraft*, vol. 5, pp. 236–242, 1968.
- [6] G. M. Callahan and A. H. Stenning, “Attenuation of inlet flow distortion upstream of axial flow compressors,” in *Proceedings of the AIAA 5th Propulsion Joint Specialist Conference*, Colo, USA, 1969.
- [7] H. Pearson and A. B. McKenzie, “Wakes in axial compressors,” *Journal of the Royal Aeronautical Society*, pp. 415–416, 1959.
- [8] C. Reid, “The response of axial flow compressor to intake flow distortion,” ASME 69-GT-29, 1969.
- [9] J. E. Calogeras, C. M. Mehalic, and P. L. Burstadt, “Experimental investigation of the effect of screen-induced total-pressure distortion on turbojet stall margin,” NASA-TM-X 2239, 1971.
- [10] E. J. Milner and L. M. Wenzel, “Performance of a J85-13 compressor with clean and distorted inlet flow,” NASA-TM-X 3304, 1975.
- [11] W. M. Braithwaite, E. J. Graber, and C. M. Mehalic, “The effect of inlet temperature and pressure distortion on turbojet performance,” AIAA 73-1316, 1973.
- [12] E. M. Greitzer and H. R. Griswold, “Compressor-diffuser interaction with circumferential flow distortion,” *Journal Mechanical Engineering Science*, vol. 18, no. 1, pp. 25–38, 1976.
- [13] L. M. Wenzel and R. J. Blaha, “Analysis of dynamic inlet distortion applied to a parallel compressor model,” NASA-TM-X 3522, 1977.
- [14] R. S. Mazzawy, “Multiple segment parallel compressor model for circumferential flow distortion,” *Journal of Engineering for Power. Transactions of the ASME*, vol. 99, no. 2, pp. 288–296, 1977.
- [15] A. Elder, “Prediction of the effect of distorted inlet flows on fan and compressor stability,” IMechE C117/84, 1984.
- [16] J. Yin and P. Pilidis, “Influence of inlet profile on high-BPR turbofan performance using a radial profile map,” in *Proceedings of the ICAS Congress*, 2002.
- [17] J. Yin, R. Hales, P. Pilidis, and B. Curnock, “2-shaft high-bypass ratio turbofan performance calculation using a new 2-D fan model,” in *Proceedings of the 37th AIAA/ASME/SAE/ASEE Joint Propulsion Conference*, Salt Lake City, Utah, USA, July 2001.
- [18] V. Pachidis, P. Pilidis, I. Templalexis, T. Korakianitis, and P. Kotsiopoulos, “Prediction of engine performance under compressor inlet flow distortion using streamline curvature,” *Journal of Engineering for Gas Turbines and Power*, vol. 129, no. 1, pp. 97–103, 2007.
- [19] V. Pachidis, P. Pilidis, F. Talhouarn, A. Kalfas, and I. Templalexis, “A fully integrated approach to component zooming using computational fluid dynamics,” *Journal of Engineering for Gas Turbines and Power*, vol. 128, no. 3, pp. 579–584, 2006.
- [20] N. L. Sanger, “Performance of a 1.57-pressure-ratio transonic fan stage with a screen-induced 90o circumferential inlet flow distortion,” NASA-TN-D 8163, 1976.
- [21] N. A. Cumpsty, *Compressor Aerodynamics*, Longman Scientific & Technical, Longman Group, UK, 1989.
- [22] J. Seddon and E. L. Goldsmith, *Intake Aerodynamics*, Collins, London, UK, 1985.
- [23] J. P. Longley and E. M. Greitzer, *Steady and Transient Performance Prediction of Gas Turbine Engines*, AGARD Lecture Series 183, Inlet Distortion Effects in Aircraft Propulsion System Integration, 1992.

- [24] V. Pachidis, *Gas turbine advanced performance simulation*, Ph.D. thesis, Cranfield University, UK, 2006.
- [25] I. Templelexis, *Turbine performance with distorted inlet flow*, Ph.D. thesis, Cranfield University, UK, 2006.
- [26] W. C. Swan, "A practical method of predicting transonic-compressor performance," *Journal of Engineering for Power*, vol. 86, pp. 322–330, 1961.
- [27] H. R. Griepentrog, "Secondary flow losses in axial compressors," *AGARD Lecture Series*, no. 39, 1970.
- [28] D. C. Urasek, W. T. Gorrell, and W. S. Cunnann, "Performance of two-stage fan having low-aspect-ratio, first-stage rotor blading," Technical Report 78-49 NASA-TP-1493, 1979.
- [29] J. F. Schmidt and R. S. Ruggeri, "Performance with and without inlet radial distortion of a transonic fan stage designed for reduced loading in the tip region," NASA-TP 1294, 1978.